

Coincidence Counting in Time-of-Flight Mass Spectrometry: A Test for Chemical Microhomogeneity

M. A. PARK, K. A. GIBSON, L. QUINONES, E. A. SCHWEIKERT*

Coincidence counting techniques have been combined with time-of-flight mass spectrometry in the examination of surfaces for chemical microhomogeneity. A mathematical formalism was developed to describe the principles underlying this coincidence counting technique and was used to produce a quantitative method for handling the data obtained. This technique of testing for chemical homogeneity has been demonstrated with a sample that consists of a physical mixture of polystyrene and crystals of NaF which were tenths of micrometers in diameter. Ultimately this approach is expected to be useful for the routine testing of surfaces for chemical homogeneity at the level of tens of nanometers.

A NOVEL APPROACH FOR TESTING the chemical homogeneity of a surface at the submicrometer level has been developed. This method combines time-of-flight (TOF) mass spectrometry with single-ion counting in the coincidence mode to determine the spatial relations of the various masses observed in a spectrum. Coincidence counting has been used almost exclusively for the determination of the chemical relations of mass spectral peaks (1–6). Although the use of coincidence counting techniques for revealing a sample's chemical homogeneity has been mentioned (7), it has not been implemented. We demonstrate that TOF mass spectrometry with coincidence counting can be used to examine the chemical microhomogeneity of a surface.

We have used the fission fragments from a ^{252}Cf source to stimulate the desorption of ions from solid samples (8). In this procedure, usually referred to as particle or plasma desorption mass spectrometry (PDMS), the desorbed sample ions, or secondary ions, are analyzed by TOF mass spectrometry and hence provide a mass spectrum of the sample. Two conditions must be met to test the chemical homogeneity of a surface: (i) the beam of incident particles should address only a small region of the sample surface at a time so that the sample components can be spatially distinguished from one another; and (ii) each component of the sample must produce a distinct mass spectral peak in order to be chemically distinguished from one another.

In our case, a single fission fragment, or primary ion, causes desorption of ions from a region on the sample of about 10 nm in diameter (9) and a few monolayers depth (10), and thus is in itself a "nanoprobe" of the sample surface. In practice, the number of secondary ions desorbed by a single primary projectile impact is too small for analytical significance (5). Instead, the TOF and coincidence spectra are generated from the accumulated secondary-ion counts from many primary ions. To take advantage of the "nanoprobe" nature of the primary particles, one need only analyze each desorption event independently. That is, the sample ions that desorb because of a given primary ion are

analyzed before the next desorption event is considered.

Several chemical components that are near each other on a surface may be excited simultaneously by an incident primary particle, hence secondary ions from adjacent components can be desorbed by the same primary particle. Ions that are detected from the same desorption event are said to be in coincidence with each other. Thus a coincidence spectrum is a spectrum composed only of counts due to secondary ions detected from desorption events that contain an ion of interest. For example, a Na^+ coincidence spectrum is composed only of counts observed as a result of those desorption events from which at least one Na^+ ion is detected. If ions of one sample component are frequently observed in coincidence with those from another, then the ions are correlated with one another and one may conclude that the components are homogeneously mixed. Alternatively, the ions are anticorrelated with one another if the component ions are rarely found in the same desorption event and one may conclude that the sample is inhomogeneous.

The PDMS setup used in this work is described in detail elsewhere (8). Briefly, secondary ions generated by a ^{252}Cf fission fragment striking a sample are accelerated by an electric field into a drift region. The flight times of the ions through the drift region are proportional to the square root of the ion's mass-to-charge ratio (m/z). The flight times of the ions through the drift region are recorded by a microcomputer through a fast timer—a multistop time-to-digital converter (TDC). The TDC used in these studies has been described elsewhere (11). In this arrangement, the microcomputer generates a normal TOF spectrum and a set of coincidence spectra from the data given it by the TDC. The normal TOF spectrum is displayed, as usual, with intensity on the ordinate and TOF on the abscissa (Fig. 1). The coincidence spectra are displayed in the form of an array that we refer to as a two-dimensional (2-D) TOF spectrum (Fig. 2).

We demonstrated the ability of the technique to discern spatial relations between sample components by preparing and analyzing a sample of NaF crystals on a spin-cast polystyrene (PS) film. Scanning electron microscopy has shown that the NaF crystals were $\sim 0.5 \mu\text{m}$ in diameter. Mass spectra were also obtained for separate samples of NaF and PS.

The spectra of the separate samples of NaF and PS are clearly different (Fig. 1). The results of the analysis of the submicrometer NaF crystals on polystyrene are shown in Figs. 2 and 3. In Fig. 2 the normal TOF spectrum appears along the diagonal,

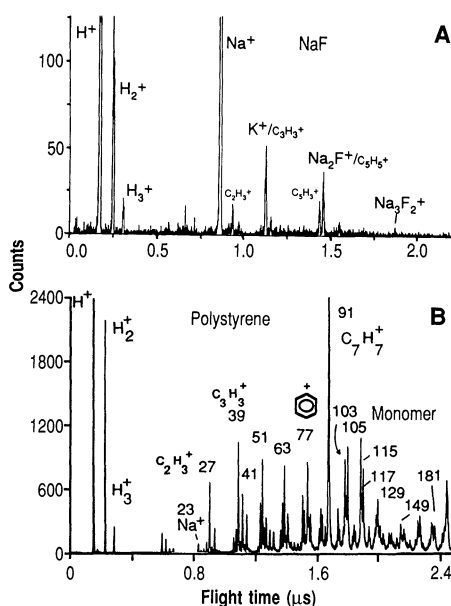


Fig. 1. Mass spectra of (A) NaF and (B) polystyrene.

Center for Chemical Characterization and Analysis, Texas A&M University, College Station, TX 77843-3144.

*To whom correspondence should be addressed.

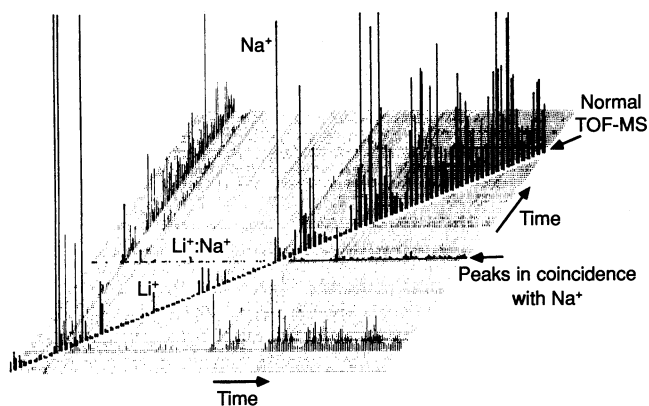


Fig. 2. A portion of the two-dimensional spectrum of about 0.5- μm diameter NaF crystals on a spin-cast polystyrene film. The “normal” spectrum along the diagonal and the Na^+ coincidence spectrum have been highlighted.

and the off-diagonal peaks correspond to coincidences between different ions. As an example, the peaks corresponding to Li^+ are clearly present. Also, the Na^+ and Na^+ in the normal spectrum are labeled as well as an off-diagonal peak corresponding to the coincidence of Li^+ and Na^+ . With such a 2-D spectrum, one can now simultaneously observe the coincidences between peaks throughout a spectrum. This capability is important in the development of a routine analysis technique because, in contrast to other acquisition systems, the coincidences throughout the spectrum can be determined relatively quickly, and when analyzing an unknown sample, one need not know what coincidences to look for before taking a spectrum.

Following data acquisition, the coincidence spectra of interest are extracted from the overall 2-D spectrum and displayed as 1-D spectra. The normal TOF spectrum of the NaF-PS sample and two relevant coincidence spectra are shown in Fig. 3. All three of these spectra were taken simultaneously. In the normal TOF spectrum of the NaF-PS

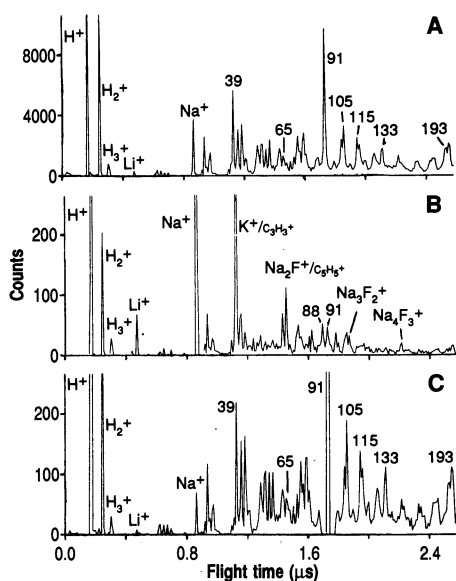


Fig. 3. Mass spectrum of (A) NaF crystals on a polystyrene film and the (B) Na^+ and (C) mass-91 coincidence spectra from the same sample.

sample (Fig. 3A), many peaks that are characteristic of PS (for example, at $m/z = 91$) and Na_2F^+ peaks are evident as well as a Li^+ contaminant. The Na^+ coincidence spectrum of the NaF-PS sample (Fig. 3B) contains (as one should expect) many of the same peaks as that of the NaF standard shown in Fig. 1A. The mass-91 coincidence spectrum (Fig. 3C) strongly resembles the spectrum of the PS standard in Fig. 1B. These similarities suggest that the peaks in coincidence with mass 91 are due to PS, whereas those in coincidence with mass 23 (Fig. 3B) are due to NaF.

Perhaps even more significant than these similarities are the differences between Figs. 3B and 3C. Even a casual inspection reveals that the PS has little influence on the Na^+ coincidence spectrum, and conversely the NaF has little influence on the mass-91 coincidence spectrum. Thus one might conclude that the PS is spatially separated from the NaF. A rigorous assessment requires the development of a quantitative model of eventwise analysis.

The concept of observing chemical inhomogeneities by coincidence counting is based on desorption probabilities. Consider a sample of dimension “ a ” square composed of compound “white” with a “black” particle of dimension “ b ” square on its surface. The sample is bombarded by high-energy ions that strike the sample surface at random locations—each ion addressing a region of the surface of dimension “ c ” square, where c is much smaller than a or b . The probability of observing a white ion if the addressed area is only white is $P(W^+)$, and the probability of observing a black ion if the addressed area is only black is $P(B^+)$.

Given such a model, one can derive the probability of observing a black ion in coincidence with a white ion due to a single fission fragment as

$$P_{\text{in}}(B^+, W^+) = (1/6)P(B^+)P(W^+)c\Delta y/a^2$$

where Δy is the length of the interface between the sample components. In con-

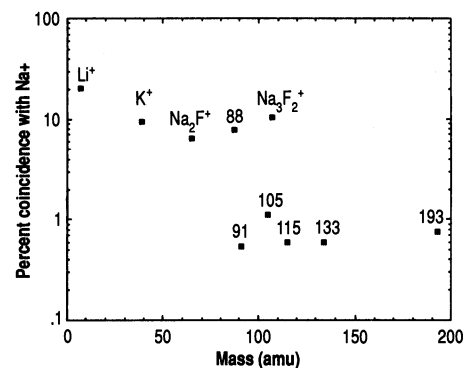


Fig. 4. A plot of percent coincidence with Na^+ versus mass. The set of points with high percent coincidence represent peaks associated with NaF, and those points with low percent coincidence are associated with PS.

trast, the probability of observing the two ions as a result of the same primary ion if the sample is chemically homogeneous is

$$P_{\text{homo}}(B^+, W^+) = \frac{P(B^+)(b^2/a^2)P(W^+)(1 - b^2/a^2)}{P(B^+)(b^2/a^2)P(W^+)(1 - b^2/a^2)}$$

In the application of this model to a set of data, one must realize that, in practice, the sample is not composed of squares but of irregularly shaped particles. These particles having a larger perimeter than squares and thus a larger interface Δy will cause the difference between $P_{\text{in}}(B^+, W^+)$ and $P_{\text{homo}}(B^+, W^+)$ to be less than predicted by the model.

These probabilities are related to the observed data through the percent coincidence of the ions. The percent coincidence of ion B^+ and W^+ is determined by dividing the number of counts in the B^+, W^+ coincidence peak, $N(B^+, W^+)$, by the total number of counts in peak B, $N(B^+)$, and multiplying the result by 100%. This is related to the desorption probabilities as

$$\%(B^+, W^+) = [N(B^+, W^+)/N(B^+)]100\%$$

The percent coincidence with the Na^+ peak for the NaF-PS sample has been plotted versus mass in Fig. 4; the peaks associated with NaF are more correlated with Na^+ than those associated with PS.

The question then arises, what difference in the percent coincidence of two peaks is required for a sample to be considered chemically inhomogeneous? One might set a criterion that this difference be, for example, at least one order of magnitude. As an example let us compare in the plot of Fig. 4, Li^+ , a contaminant in the NaF, and mass 91, the major fragment ion produced from PS. The plot shows Li^+ as having 20% coincidence with Na^+ , whereas mass 91 has only 0.5% coincidence with Na^+ . Since the percent coincidence of Li^+ with Na^+ is about 40 times that of mass 91 with Na^+ ,

we conclude that the sample is chemically inhomogeneous, that the Li^+ comes from the same source as Na^+ , and that the mass-91 ions come from a different source than either Na^+ or Li^+ . This same argument holds for several other species as well. The peaks associated with PS generally have <1% coincidence with Na^+ whereas those associated with NaF have >5% coincidence with Na^+ (Fig. 4).

For a more precise comparison between the two groups, one can also attempt to fit the experimental data to the model. Given that the sample is composed of $\sim 0.5\text{-}\mu\text{m}$ NaF crystals on PS and that the coverage of these crystals on the PS surface is $\sim 3\%$, one finds that $P_{\text{homo}}(\text{M}^+, \text{Na}^+)$, where M^+ is an arbitrary mass ion, is a factor of ~ 70 greater than $P_{\text{in}}(\text{M}^+, \text{Na}^+)$. In Fig. 4, $P_{\text{in}}(\text{M}^+, \text{Na}^+)$ is represented by the group of points associated with PS, whereas $P_{\text{homo}}(\text{M}^+, \text{Na}^+)$ is represented by the group of points associated with NaF. From the plot, one observes that $\%_{\text{homo}}(\text{M}^+, \text{Na}^+)$ is only a factor of 15 greater than $\%_{\text{in}}(\text{M}^+, \text{Na}^+)$. This factor is lower than that predicted by the model because the NaF crystals are not squares as the model assumes. As noted earlier, irregularly shaped NaF crystals lead to a longer interface between the NaF and the PS and larger values for $\%_{\text{in}}(\text{M}^+, \text{Na}^+)$ than are expected by the model. Nevertheless, the difference in the percent coincidences of more than an order of magnitude between the two groups supports the conclusion that the polystyrene is indeed spatially well separated from the NaF.

This example demonstrates the use of coincidence counting with TOF mass spectroscopy in the analysis of surfaces for chemical homogeneity at the 100-nm level. In principle, the technique should have an ultimate resolution of about 10 nm, that is, the diameter of the sample spot addressed by an individual primary ion (9). In practice, the resolution limit is set by the length of the interface of highly irregularly shaped inhomogeneities in the sample. The coincidence spectra may also be useful in revealing chemical relations between secondary ions and in the separation of mass spectrometric signal from background. Further, coincidence counting may be useful in examining the kinetic energy relations of secondary ions and the relation of secondary ions to secondary electrons.

REFERENCES AND NOTES

1. L. Schmidt and H. Jungclas, *Lect. Notes Phys.* **269**, 234 (1986).
2. A. Hedin, P. Hakansson, B. U. R. Sundqvist, *Int. J. Mass Spectrom. Ion Processes* **77**, 123 (1987).
3. N. Furstenua, *Z. Naturforsch.* **33a**, 563 (1978).
4. ———, W. Knippelberg, F. R. Krueger, G. Weiss, K. Wien, *ibid.* **32a**, 711 (1977).
5. R. D. Macfarlane, *Anal. Chem.* **55**, 1247A (1983).
6. L. Q. Huang, R. J. Conzemius, G. A. Junk, R. S. Houk, *Int. J. Mass Spectrom. Ion Processes* **90**, 85 (1989).
7. S. Della Negra, D. Jacquet, I. Lorthiois, Y. Le Beyec, *Int. J. Mass Spectrom. Ion Phys.* **53**, 215 (1983).
8. W. R. Summers and E. A. Schweikert, *Rev. Sci. Instrum.* **57**, 692 (1986).
9. K. Wien, *Lect. Notes Phys.* **269**, 1 (1986).
10. G. Bolbach *et al.*, *Nucl. Instrum. Methods Phys. Res.* **B30**, 74 (1988).
11. E. Festa and R. Sellem, *Nucl. Instrum. Methods* **188**, 99 (1981).
12. We thank C. H. Spiegelman of the Department of Statistics at Texas A&M University for consultation on the statistical models described above.

12 December 1989; accepted 4 April 1990

Image Reconstruction of the Interior of Bodies That Diffuse Radiation

J. R. SINGER, F. ALBERTO GRÜNBAUM, PHILIP KOHN,
JORGE PASSAMANI ZUBELLI

A method for reconstructing images from projections is described. The unique aspect of the procedure is that the reconstruction of the internal structure can be carried out for objects that diffuse the incident radiation. The method may be used with photons, phonons, neutrons, and many other kinds of radiation. The procedure has applications to medical imaging, industrial imaging, and geophysical imaging.

IN THIS REPORT WE DESCRIBE A PROCEDURE to determine and display images of the internal structure of objects that diffuse radiation. Such objects are members of a large class. For example, the human body diffuses infrared radiation, ultrasonic radiation, and neutrons. Almost all solids are also in this class. It is difficult to specify a substance in which diffusion along with absorption does not occur for some form of radiation.

We began studying the transmission of infrared laser beams through animal tissues. The projections of diffusely transmitted radiation could be observed by silicon detector arrays and displayed on a video screen. For tissues up to about 2 cm thick, we could observe shadowgraphs of internal structures. Thicker tissues produced fuzzier shadowgraphs until the internal structures became difficult to delineate. Conventional techniques for reconstructing multiple projections by Cormack (1), Hounsfield (2), Boyd (3), and others for application to computer tomography were not helpful in reconstructing our diffused projections. We did observe that considerable information about internal structures existed within these projections. This observation prompted our research into methods of reconstructing internal images of objects utilizing a large collection of shadowgraphs.

The problem was to develop a method of image reconstruction that could utilize the diffused image projections and reconstruct

internal features of the diffusing object. The simplest case is a homogeneous slab with no internal structure with a particle beam directed at the face of the slab. This ideal example has been completely solved by Feynman and Hibbs (4). However, imaging the interior of a homogeneous body provides minimal information because there is no interior structure. In imaging more complex objects, we use the Feynman concept of summing the emergent particles over all possible paths (5). The resultant pattern of emergent particles will therefore contain the "history" of these paths.

To reconstruct the interior structure of an object containing inhomogeneities, we make the following assumptions:

1) Divide the object into volume elements (voxels); set the size of the voxels to be the desired resolution. (When dealing with the two-dimensional case, each element is termed a pixel.)

2) The particle beam enters the object at a series of points sequentially in time.

3) The particles of the beam may enter and leave each voxel, if not annihilated by absorption within the voxel. The absorption probability is ν_{ijk} per voxel, and the survival probability is w_{ijk} per voxel, where $w_{ijk} = 1 - \nu_{ijk}$. The scattered probabilities for each voxel are f_{ijk} = forward scatter probability, b_{ijk} = backward scatter probability, s_{ijk} = sideways scatter probability, and we assume that $b_{ijk} = 1 - 4s_{ijk} - f_{ijk}$. The probability of a forward scatter is given by $w_{ijk} \cdot f_{ijk}$; the probability of a backward scatter is $w_{ijk} \cdot b_{ijk}$; the probability of a sideways scatter is $w_{ijk} \cdot s_{ijk}$.

4) For each voxel we provide the variables w , f , b , and s . As pointed out above, these reduce to three variables.

J. R. Singer, Electrical Engineering and Computer Science, and Biophysics Departments, University of California, Berkeley, CA 94720.
F. A. Grünbaum and J. P. Zubelli, Mathematics Department, University of California, Berkeley, CA 94720.
P. Kohn, International Computer Sciences Institute, University of California, Berkeley, CA 94720.